AGU PUBLICATIONS

JGR

Journal of Geophysical Research: Atmospheres

RESEARCH ARTICLE

10.1002/2013JD020838

Roles of transport and chemistry processes in global ozone change on interannual and multidecadal time scales

T. Sekiya[1] **and K. Sudo**[1]

[1]Graduate School of Environmental Studies, Nagoya University, Nagoya, Japan

Key Points:
- Roles of transport and chemistry in ozone changes are investigated
- Transport and chemistry play important roles in ENSO-related ozone variation
- Future change in tropospheric ozone is caused by transport as well as chemistry

Supporting Information:
- Readme
- Text S1.doc
- Table S1.txt
- Table S2.txt
- Table S3.txt
- Figure S1.eps
- Figure S2.eps
- Figure S3.eps
- Figure S4.eps
- Figure S5.eps
- Figure S6.eps

Correspondence to:
T. Sekiya,
tsekiya@nagoya-u.jp

Citation:
Sekiya, T., and K. Sudo (2014), Roles of transport and chemistry processes in global ozone change on interannual and multidecadal time scales, *J. Geophys. Res. Atmos.*, *119*, 4903–4921, doi:10.1002/2013JD020838.

Received 5 SEP 2013
Accepted 21 MAR 2014
Accepted article online 25 MAR 2014
Published online 17 APR 2014

Abstract This study investigates ozone changes and the individual impacts of transport and chemistry on those changes. We specifically examine (1) variation related to El Niño Southern Oscillation, which is a dominant mode of interannual variation of tropospheric ozone, and (2) long-term change between the 2000s and 2100s. During El Niño, the simulated ozone shows an increase (1 ppbv/K) over Indonesia, a decrease (2–10 ppbv/K) over the eastern Pacific in the tropical troposphere, and an increase (50 ppbv/K) over the eastern Pacific in the midlatitude lower stratosphere. These variations fundamentally agree with those observed by Microwave Limb Sounder/Tropospheric Emission Spectrometer instruments. The model demonstrates that tropospheric chemistry has a strong impact on the variation over the eastern Pacific in the tropical lower troposphere and that transport dominates the variation in the midlatitude lower stratosphere. Between the 2000s and 2100s, the model predicts an increase in the global burden of stratospheric ozone (0.24%/decade) and a decrease in the global burden of tropospheric ozone (0.82%/decade). The increase in the stratospheric burden is controlled by stratospheric chemistry. Tropospheric chemistry reduces the tropospheric burden by 1.07%/decade. However, transport (i.e., stratosphere-troposphere exchange and tropospheric circulation) causes an increase in the burden (0.25%/decade). Additionally, we test the sensitivity of ozone changes to increased horizontal resolution of the representation of atmospheric circulation and advection apart from any aspects of the nonlinearity of chemistry sensitivity to horizontal resolution. No marked difference is found in medium-resolution or high-resolution simulations, suggesting that the increased horizontal resolution of transport has a minor impact.

1. Introduction

Ozone, the third most important greenhouse gas for the period from the pre-Industrial era to the present, is also an air pollutant near the surface and a shield against ultraviolet radiation in the stratosphere [*Forster et al.*, 2007]. In addition, stratospheric and tropospheric ozone partly affect changes in tropospheric circulation. Tropospheric jets in the Southern Hemisphere are influenced by changes in stratospheric ozone over the Antarctic [e.g., *Son et al.*, 2008, 2010; *Eyring et al.*, 2013a]. Latitudinally dependent heating attributable to tropospheric ozone and black carbon may have caused expansion of the tropics in the Northern Hemisphere during the last three decades [*Allen et al.*, 2012]. Therefore, examination of future changes in stratospheric and tropospheric ozone distribution is important to evaluate the effect of ozone on climate change.

Meteorological variability plays a crucial role in interannual variation in stratospheric and tropospheric ozone distribution [e.g., *Hess and Mahowald*, 2009; *Eyring et al.*, 2010a; *Pozzoli et al.*, 2011]. El Niño Southern Oscillation (ENSO) is a dominant mode of interannual variation in ozone in the troposphere. The earliest study of it analyzed tropical tropospheric ozone changes during the 1997 El Niño (the positive phase of ENSO) using Total Ozone Mapping Spectrometer instruments [*Chandra et al.*, 1998]. Analysis of long-term ozonesonde and satellite data revealed ozone changes related to ENSO in the troposphere [*Ziemke and Chandra*, 1999; *Ziemke et al.*, 2010; *Randel and Thompson*, 2011]. Recent studies using satellite instruments (Microwave Limb Sounder (MLS) and Tropospheric Emission Spectrometer (TES) aboard Aura) observed vertically resolved ozone changes associated with ENSO [*Oman et al.*, 2013]. Many modeling studies have demonstrated that the observed tropospheric ozone change associated with ENSO was reproduced in simulations forced by the assimilated meteorology [*Sudo and Takahashi*, 2001; *Chandra et al.*, 2002, 2009; *Nassar et al.*, 2009], and in simulations forced by the observed sea surface temperature variability [*Doherty et al.*, 2006; *Oman et al.*, 2011, 2013]. *Sudo and Takahashi* [2001], *Chandra et al.* [2002], *Doherty et al.* [2006],

and *Nassar et al.* [2009] have also suggested that meteorological condition changes play a crucial role in the large-scale variation in tropospheric ozone and that anomalous wildfires cause increased tropospheric ozone over Indonesia. *Sudo and Takahashi* [2001] reported that the key meteorological factors are upward versus downward motion, enhanced versus suppressed convection, and their associated water vapor changes. Furthermore, satellite and ozonesonde observations showed a negative anomaly of ozone above the tropical tropopause, and positive anomalies in the lower stratosphere over approximately 30°–50°N and S during the positive phase of ENSO over the past few decades [e.g., *Randel et al.*, 2009; *Randel and Thompson*, 2011]. *Randel et al.* [2009] demonstrated that a chemistry-climate model reproduced those anomalies of the stratospheric ozone. These ozone changes are related to an acceleration of the Brewer-Dobson circulation during the positive phase of ENSO [*Calvo et al.*, 2010].

Tropospheric ozone has increased from the pre-Industrial era to the present because of increased emissions of tropospheric ozone precursors (NO_x, CO, nonmethane VOCs) and methane [*Fusco and Logan*, 2003; *Lang et al.*, 2012; *Stevenson et al.*, 2013]. Stratospheric ozone has been depleted over the past three decades, which is attributable to increased emissions of ozone-depleting substances (ODSs) [*Gillett et al.*, 2011]. In the future, both emissions and climate change are expected to influence changes in stratospheric and tropospheric ozone [*Brasseur et al.*, 2006; *Zeng et al.*, 2008; *Eyring et al.*, 2010b; *Kawase et al.*, 2011]. Future changes in stratospheric ozone are expected to be influenced by a decrease in temperature and by a strengthening of the Brewer-Dobson circulation associated with climate change [*Li et al.*, 2009]. In the troposphere, the strengthening also increases tropospheric ozone through stratosphere-troposphere exchange (STE) of ozone [e.g., *Collins et al.*, 2003; *Sudo et al.*, 2003; *Zeng and Pyle*, 2003]. In the lower troposphere, higher water vapor facilitates the chemical destruction of tropospheric ozone [*Johnson et al.*, 2001]. Moreover, higher temperature decomposes PAN into NO_x more efficiently [e.g., *Doherty et al.*, 2013]. Recent studies have also investigated the future changes under the framework of multimodel intercomparison projects [*Stevenson et al.*, 2006; *Eyring et al.*, 2010a, 2013a; *Young et al.*, 2013].

This study quantifies the individual impacts of transport and chemical processes on the ozone changes on two time scales. We specifically examine (1) variation related to El Niño Southern Oscillation (ENSO), which is a dominant mode of interannual variation of tropospheric ozone, and (2) long-term change between the 2000s and 2100s. *Sekiya and Sudo* [2012] assessed the individual impact on the ENSO-related variation in tropospheric ozone. The present study further investigates the individual impacts on the ENSO-related variation in vertical ozone distribution from the lower troposphere to the lower stratosphere. Regarding the long-term change in stratospheric and tropospheric ozone, previous studies investigated a response of ozone to an individual external forcing (e.g., tropospheric ozone precursors, ODSs, and GHGs). We must also investigate the role of the individual process quantitatively.

Additionally, we test sensitivities of the ENSO-related variation and the future changes in ozone to increased horizontal resolution of the representation of atmospheric circulation and advection apart from chemistry using the model with two horizontal resolutions (about 300 km and 120 km). Therefore, this study does not consider an impact of horizontal resolution change on the nonlinearity of the ozone chemistry in the stratosphere and troposphere. Earlier studies have typically used chemistry-climate models (CCMs) with about 300 km horizontal resolution. Nevertheless, it remains unclear whether such CCM resolution simulates the variation and change appropriately.

This paper is organized as follows. Section 2 provides the model description, experimental settings, and observational data. We compare the present-day simulation with observations in section 3. In section 4, we evaluate ENSO-related variation of ozone during 2004–2009 by comparison with satellite and ozonesonde observations. Section 5 shows future projections of ozone in the troposphere and lower stratosphere. Finally, in section 6, we summarize the results and present our conclusions.

2. Methodology

2.1. Model Description

This study used two version of MIROC-ESM-CHEM [*Watanabe et al.*, 2011a]: (1) an atmospheric general circulation model (AGCM) version which includes full-chemistry processes, (2) an O_3-tracer-transport (tagged-tracer) model version [*Sudo and Akimoto*, 2007]. The AGCM version was used to archive the production rate (P) and loss frequency (β) of O_x family. The family is defined as a sum of O_3, $O(^1D)$, and O. The O_3-tracer-transport model version was driven by the archived P and β from the AGCM version. This version

was applied to quantify individual contributions of transport and chemical processes to ozone changes and to test a sensitivity of ozone changes to increased horizontal resolution of ozone transport.

The AGCM version is an atmospheric component of the original version of MIROC-ESM-CHEM which includes atmosphere, ocean, and land surface models (i.e., an earth system model). The model used for this study consists only of AGCM coupled with a Spectral Radiation-Transport Model for Aerosol Species (SPRINTARS) aerosol model [*Takemura et al.*, 2005] and a CHemical AGCM for Studies of atmospheric Environment and Radiative forcing (CHASER) atmospheric chemistry model [*Sudo et al.*, 2002; *Sudo and Akimoto*, 2007]. The sea surface temperature (SST) and sea ice concentration (SIC) in the model are prescribed as boundary conditions. We adopt a horizontal resolutions of T42 (about 2.8° × 2.8°) with 57 vertical layers from the surface to about 52 km altitude. The vertical resolution increases to 1000 m per level from the surface to 5 km, decreases again to 680 m per level from 5 km to 8 km, remains constant (680 m per level) for 8–35 km, and increases to 3500 m per level above 35 km. Tracer transport in the model is simulated using the piecewise parabolic method [*Colella and Woodward*, 1984] and the flux-form semi-Lagrangian scheme [*Lin and Rood*, 1996] on a grid scale. The model also incorporates tracer transport on a subgrid scale (convective transport and vertical turbulence mixing). The model uses fourth-order (∇^4) horizontal hyperviscosity diffusion. The *e*-folding time of the smallest resolved wave is 1.3 days for the T42 simulation. Although the model incorporates the *McFarlane* [1987] orographic gravity wave parameterization, no nonorographic gravity wave parameterization is included.

CHASER simulates details of photochemistry in the troposphere and the stratosphere, chemical tracer transport, wet and dry deposition, and emissions. In this study, the model incorporates 93 species and 263 reactions (58 photolytic, 184 kinetic, and 21 heterogeneous reactions), including the chemical cycle of O_x-NO_x-HO_x-CH_4-CO with volatile organic carbons (VOCs) oxidation and halogen (Cl and Br) chemistry. All chemical reactions are calculated in the troposphere and the stratosphere. In the scheme of chemical reactions, the P and β of O_x family are simultaneously archived. The P is defined as the total production rate of O_x by the following reactions: $NO_2 + h\nu \rightarrow NO + O$, $O_2 + h\nu \rightarrow 2O$, and the other 9 reactions. Moreover, the β is the total loss frequency of O_x by the following reactions: $O_3 + O \rightarrow 2O_2$, $O(^1D) + H_2O \rightarrow 2OH$, the reactions of O_x with HO_x, NO_x, Cl, and Br radicals, and the other 29 reactions. In the troposphere, wet deposition (rain out and wash out) is calculated in the framework of cumulus convection and large-scale condensation schemes in the AGCM. The model also calculates dry deposition [*Wesely*, 1989] at the surface. Lightning NO_x production is calculated in the framework of cumulus convection scheme in the AGCM. This scheme calculates the global lightning NO_x production of about 5.2 Tg N/year for the 2000s. In the stratosphere, the model simulates formation of the polar stratospheric cloud, its gravitational settling, and heterogeneous reactions on it. The model uses the scheme adopted at the Center of Climate System Research/National Institute of Environmental Studies (NIES) stratospheric chemistry-climate model [*Nagashima et al.*, 2002; *Akiyoshi et al.*, 2004]. Additional information of MIROC-ESM-CHEM can be found in *Watanabe et al.* [2011a].

The O_3-tracer-transport model version was used to quantify individual contributions of transport and chemical processes to ozone changes and to test a sensitivity of ozone changes to increased horizontal resolution of transport representation. Atmospheric dynamical and physical processes in the model are identical to those in the original version of MIROC-ESM-CHEM. The ozone tendency at each grid is written as

$$\frac{dC}{dt} = \left(\frac{dC}{dt}\right)_{\text{transport}} + \left(\frac{dC}{dt}\right)_{\text{dry deposition}} + P - \beta C, \quad (1)$$

where C stands for the ozone concentration in the O_3-tracer-transport model version and where subscripts denote processes. The model calculates the ozone tendency attributable to transport and dry deposition processes (first and second term) in the same way as the original version, although the P and β are prescribed by the output obtained from the AGCM version of MIROC-ESM-CHEM which includes full chemistry in CHASER. The P and β at each time step are linearly interpolated from the three hourly mean outputs of P and β. A simulated value in the O_3-tracer-transport model version does not exactly match that in the AGCM version (including full chemistry). However, those versions with the same initial condition show similar results (section 3). Using the model with T42 (2.8° × 2.8°) and T106 (1.1° × 1.1°) horizontal resolutions, we test the sensitivity of changes in stratospheric and tropospheric ozone to changes in horizontal resolution. For the T106 model, the *e*-folding time of the smallest resolved wave is 0.9 days. The P and β for the T106 model are linearly interpolated from the P and β for the T42 model. To test the impact of the interpolation method, we compare the T106 simulations in which two types of P and β are prescribed. One is linearly

Table 1. Summary of Experiment Performed in This Study

Full-Chemistry Simulation (FC)

Period	SST/SIC	GHGs/ODSs/Emissions
2000s (5 years)	HadISST[a]	Historical (2000)
2100s (5 years)	HadISST[a] + MIROC[b]	Representative Concentration Pathway6 (2100)
2004–2009	HadISST	Historical (2000)

[a]Average for 1995–2004.
[b]Difference between the 2000s and 2100s simulated by MIROC-ESM-CHEM.

interpolated. The other is calculated using the area-weighted interpolation. The results of comparison suggest that the difference of ozone attributable to the interpolation method is less than that attributable to the meteorological field (see the supporting information). Because the P and β for the T106 model is calculated from those for the T42 model, this study does not consider an impact of horizontal resolution on the nonlinearity of the ozone chemistry in the stratosphere and the troposphere.

2.2. Experiments

We performed time-slice runs for the 2000s and the 2100s, which mean an average state in the years around 2000 and 2100, respectively. We compare the time-slice run for the 2000s with satellite and ozonesonde observations. The time-slice runs are also used to investigate future change in stratospheric and tropospheric ozone between the 2000s and 2100s. A transient run for 2004–2009 was also performed. We evaluate ENSO-related variation in stratospheric and tropospheric ozone during 2004–2009 in the transient run. To obtain boundary conditions (chemical production and loss rate of O_x family, N_2O, CH_4, and CFCs) for the O_3-tracer-transport model version, we conducted simulations using the AGCM version with T42 resolution (hereinafter FC). Subsequently, we performed simulations using the O_3-tracer-transport model version with T42 and T106 resolutions (hereinafter MTT and HTT, respectively). In this study, we, respectively, refer to T42 and T106 as medium and high horizontal resolution. The simulation settings used for this study are presented in Tables 1 and 2.

2.2.1. Time-Slice Simulation

We conducted time-slice FC simulations for the 2000s and the 2100s. Their lengths are 5 years in each period. The simulation lengths in this study are the same as *Zeng et al.* [2008] and within the range of the Atmospheric Chemistry and Climate Model Intercomparison Project (ACCMIP) time-slice simulations (4–14 years) [*Lamarque et al.*, 2013]. Initial conditions were taken from the result of ACCMIP experiment for the corresponding period using MIROC-ESM-CHEM because CH_4 and N_2O concentrations in the experiments are in equilibrium state under the condition in each period. We specified the concentrations of greenhouse gases (GHGs) and ODSs in 2000 [*Meinshausen et al.*, 2011], and the emissions of tropospheric ozone precursors in 2000 [*Lamarque et al.*, 2010] as the boundary conditions for the 2000s (Table 1). The average of HadISST data [*Rayner et al.*, 2003] for 1995–2004 was used as the SST/SIC for the 2000s. The biogenic emissions of isoprene and terpenes estimated by *Guenther et al.* [1995] were reduced, respectively, by 20% to 400 Tg C/year and 100 Tg C/year following *Houweling et al.* [1998] and *Roelofs and Lelieveld* [2000]. We used the monthly mean climatology of biogenic emissions because this study examines a combined impact of anthropogenic and biomass burning emissions and climate change on stratospheric and tropospheric ozone. We chose the RCP6 scenario [*Masui et al.*, 2011] as the concentrations of GHGs and ODSs and the emissions of

Table 2. Summary of Experiment Performed in This Study

O_3-Tracer-Transport Simulation

Experiment	Horizontal Resolution	Period	SST/SIC	P, β
MTT	T42	2000s (7 years) 2100s (7 years) 2004–2009	HadISST[a] HadISST[a] + MIROC[b] HadISST	2000s 2100s 2004–2009
HTT	T106	2000s (7 years) 2100s (7 years) 2004–2009	HadISST[a] HadISST[a] + MIROC[b] HadISST	2000s 2100s 2004–2009
MTT-fCHEM	T42	2100s (7 years) 2004–2009	HadISST[a] + MIROC[b] HadISST	2000s average for 2004–2009

[a]Average for 1995–2004.
[b]Difference between the 2000s and 2100s simulated by MIROC-ESM-CHEM.

tropospheric ozone precursors in 2100. The monthly mean anomalies of SST between the 2000s and 2100s in the original version of MIROC-ESM-CHEM [*Watanabe et al.*, 2011b] added to the SST for the 2000s were used as the SST for the 2100s. The SIC for the 2100s was prescribed in the same manner.

We conducted time-slice MTT simulations for the 2000s and the 2100s. The simulations were conducted for 7 years in each period. The P, β, and GHGs (N_2O, CH_4, and CFCs) were prescribed by the output obtained from the time-slice FC simulations (Table 2). The other settings were the same as the time-slice FC simulations. Additionally, we performed a simulation that calculates the ozone tendency attributable to transport and dry deposition with the 2100s boundary condition and the ozone tendency attributable to chemistry with the 2000s boundary condition (hereinafter MTT-fCHEM). To assess the sensitivity of the future change in ozone to the change in horizontal resolution, we performed time-slice HTT simulations for the 2000s and the 2100s. Their lengths were 7 years in each period. The boundary and initial conditions for the time-slice HTT simulations were linearly interpolated from those for the MTT simulations.

2.2.2. Transient Simulation

We conducted transient FC, MTT, and HTT simulations during 2004–2009 with the SST/SIC in the corresponding year (Tables 1 and 2). The other settings were the same as those of the time-slice simulations for the 2000s. This study also performed transient MTT-fCHEM simulation, which maintained the P and β at the average for 2004–2009 and which allowed the ozone tendency because of transport and dry deposition to vary among years. However, the P and β for the MTT-fCHEM simulation accompanied diurnal and seasonal cycles which were averaged during 2004–2009.

2.3. Observation Data

We used data derived from Microwave Limb Sounder (MLS) and Tropospheric Emission Spectrometer (TES) instruments for evaluation of the stratospheric and tropospheric ozone in the model. The MLS/TES data were constructed following *Oman et al.* [2013]. MLS level 2 version 3.3 data were used for ozone above 261 hPa. The data were screened using the quality and convergence threshold recommended by *Livesey et al.* [2011]. We used TES level 3 version 2 monthly mean data for ozone below 261 hPa. TES ozone profiles have about 2 degrees of freedom for signals in the troposphere [e.g., *Worden et al.*, 2004]. The MLS and TES data were mapped into the model grid. *Oman et al.* [2013] used the MLS data from August 2004 to May 2012 and the TES data from September 2004 to December 2009 because the frequency of TES observations decreased after January 2010. However, we used data from September 2004 to December 2009, when both MLS and TES are available. In this study, the averaging kernels of MLS and TES were not applied to the simulated ozone.

We also used ozonesonde data for comparison with the simulations for the 2000s (section 3). We applied the ozonesonde data compiled by *Tilmes et al.* [2012], which are climatological data of 42 selected stations for 1995–2011. We also acquired monthly mean data obtained at Samoa, Java, and Hilo for 2004–2009 obtained from Southern Hemisphere Additional Ozonesondes (SHADOZ) [*Thompson et al.*, 2003a, 2003b, 2007]. Those data were used for evaluation of the simulated variation in ozone associated with ENSO (section 4).

3. Evaluation of Present-Day Ozone

We first compare ozone in the simulation for the 2000s with that in the observational data before investigating the ENSO-related variation and the future change in ozone. The simulated ozone volume mixing ratio is compared with the MLS/TES data and the ozonesonde observations. Figure 1a shows the annual and zonal mean ozone in the MLS/TES observation averaged for the period during 2005–2009. General features of the observed distribution are reproduced by the FC, MTT, and HTT simulations (contour in Figures 1b–1d). Figures 1b–1d also show differences between the observed and the simulated ozone in the stratosphere and troposphere. The difference is within 10% in the middle and upper stratosphere (1–20 hPa). However, the simulated ozone in the lower stratosphere is high biased to that in the MLS/TES observation (10–30% in 20–50 hPa and 30–60% in 50–200 hPa). In contrast, the simulated ozone in the middle troposphere is low biased (15–40%). In the upper stratosphere, the FC simulation shows a negative bias which is not seen in the MTT and HTT simulations. This difference reflects the difference of the model version. The FC simulation (the AGCM version) calculates O_3, while the MTT and HTT simulations (the O_3-tracer transport model version) calculate O_x tracer.

Figures 2a–2d show biases of ozone in the simulations and the MLS/TES observation relative to that in the ozonesonde observation. Each panel of Figure 2 shows the average of all available profiles at the stations,

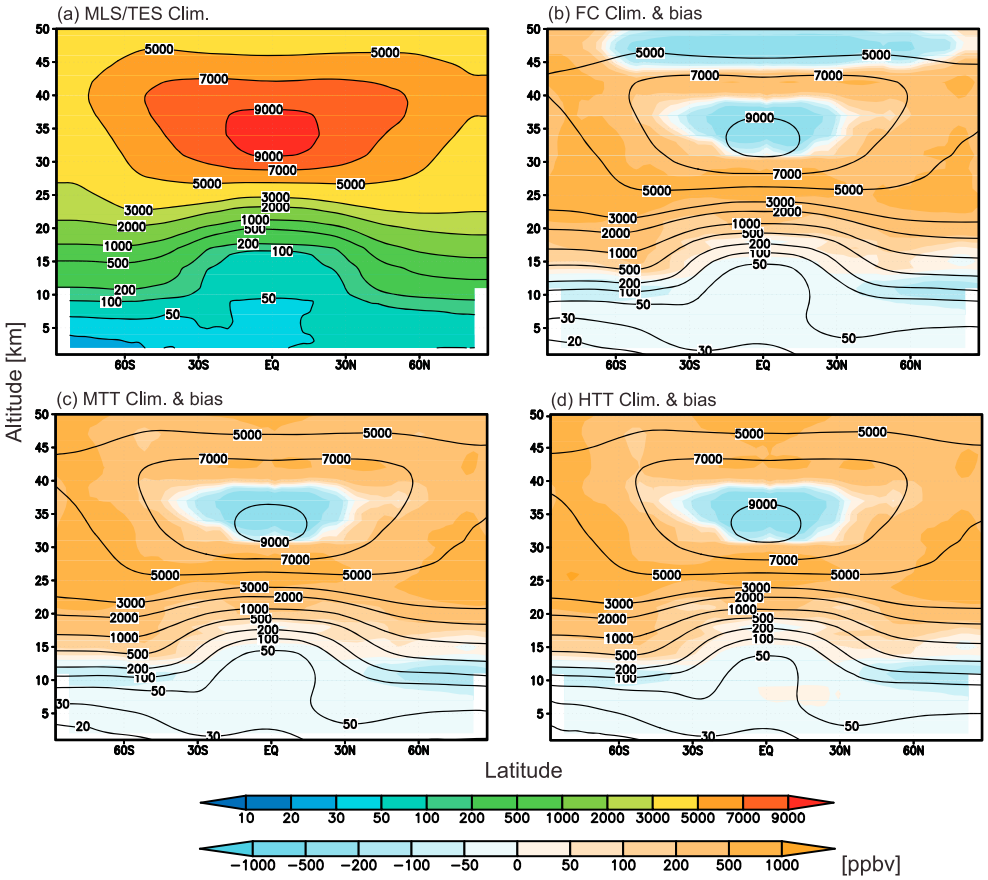

Figure 1. Annual and zonal mean ozone (ppbv). (a) The mean value during the period 2005–2009 observed by the MLS/TES instruments. (b–d) The mean in the simulations for the 2000s (contour) and its bias relative to that derived from the MLS/TES instruments (shading). Figures 1b–1d, respectively, denote the FC simulation, the MTT simulation, and the HTT simulation.

which are located in the corresponding latitude band. The ozone profiles in the simulations and the MLS/TES observation are sampled at the closest grid to the station. Although the bias of ozone observed by the MLS/TES instruments is within 10% compared to that observed by the ozonesonde in the stratosphere, it is high biased by 50% in the troposphere. The simulated ozone in the MTT is high biased to that

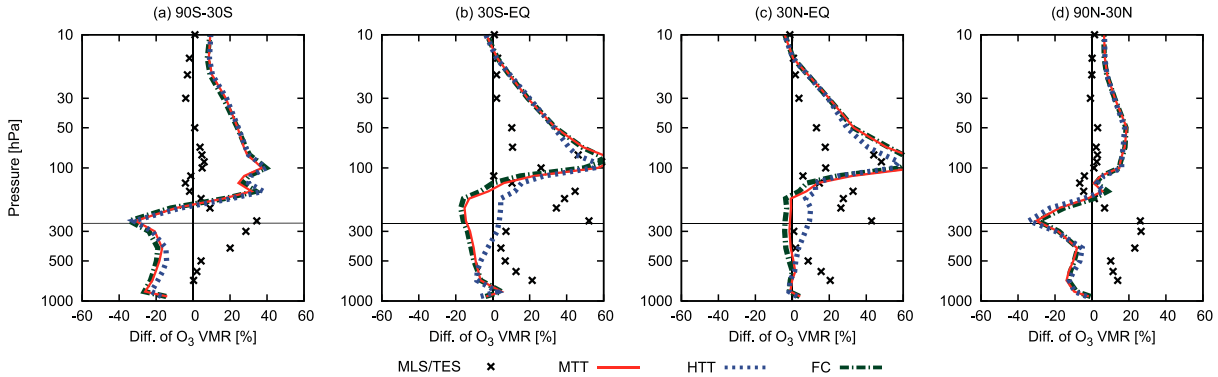

Figure 2. Biases of ozone in the MLS/TES measurements and the simulations relative to that in the ozonesonde observations (%) for the 2000s. Each panel shows the average of all available profiles in (a) 90°S–30°S, (b) 30°S–equator, (c) equator–30°N, and (d) 30°N–90°N. The black crosses show the MLS/TES observation averaged for 2005–2009. The green dash-dotted line, the red solid line, and the blue dotted line, respectively, show the simulated ozone in the FC simulation, the MTT simulation, and the HTT simulation for the 2000s. The MLS and TES data are displayed, respectively, above and below the horizontal dashed black line. The ozonesonde data averaged for 1995–2011 were compiled by *Tilmes et al.* [2012].

in the ozonesonde by 30% above 50 hPa. The simulated ozone shows a positive bias larger than 50% at altitudes between the tropopause and 50 hPa. The bias near the tropopause is attributable to the simulated tropopause height, which is lower than the observed one, because such large bias near the tropopause in the MTT simulation is not found on the height coordinate relative to the tropopause. The tropopause is determined from temperature lapse rate using the WMO definition [*WMO*, 1957]. In contrast, the tropospheric ozone in the simulations is low-biased to that in the ozonesonde by 30%. The FC simulation shows biases similar to the MTT simulation in the all latitude bands at altitudes between 1000 hPa and 10 hPa. The simulated tropospheric ozone in the HTT simulation is similar to that in the MTT simulation in the extratropics. In the tropics, tropospheric ozone in the HTT simulation is larger compared to that in the MTT simulation (Figures 2b and 2c). The increase reduces the bias in the southern tropics, although it raises the bias in the northern tropics. The results of the MTT simulation are generally similar to those of the FC simulation (Figures 1b and 2). Therefore, we present only the results of the MTT and HTT simulations hereinafter.

4. ENSO-Related Variation

This study evaluates ENSO-related ozone variation in the simulations forced by the observed SST variability with that derived from the MLS/TES instruments and the SHADOZ ozonesonde network. The observed variation related to ENSO was found by *Randel and Thompson* [2011] and *Oman et al.* [2011, 2013]. Additionally, we test the sensitivity of the ozone variation to increased horizontal resolution using the simulations with medium (about 300 km) and high (about 120 km) resolutions. The interannual variation of ozone in the lower stratosphere is influenced by the quasi-biennial oscillation (QBO) as well as ENSO [e.g., *Randel and Wu*, 2007; *Oman et al.*, 2013]. Therefore, we used multiple linear regression analysis to assess the ENSO-related variation in ozone in the MLS/TES observation and the HTT simulation as

$$C(t) = \sum_i a_i X_i(t) + \varepsilon(t). \tag{2}$$

Therein, C is an anomaly of ozone, a represents the partial regression coefficient, X denotes indices of ENSO and QBO, and ε stands for a residual term. The Niño3.4 index was used as the index of ENSO. The Niño3.4 index was calculated from the HadISST data. Two orthogonal time series based on empirical orthogonal function analysis of zonal wind at equator were used as the QBO indices [*Wallace et al.*, 1993; *Randel and Wu*, 1996]. The QBO indices for the MLS/TES observation and the HTT simulation were calculated, respectively, from the zonal wind field in the ERA-Interim data and the HTT simulation. Linear regression analysis was applied for the MTT simulation because the MTT simulation does not internally generate QBO. This analytical method resembles that used in *Oman et al.* [2011, 2013].

We analyze the simulation during 2004–2009 to evaluate the simulated ozone variation related to the observed SST variability during the same period as that of the observation. However, the simulation length is shorter than that in the previous studies [e.g., *Doherty et al.*, 2006; *Oman et al.*, 2011, 2013]. We present the 3 month running mean of the Niño3.4 index, the anomaly of ozone in the MTT and HTT simulations (Figure 3). In the MTT and HTT simulations, the simulated anomaly of ozone is well correlated with the Niño3.4 index at 3 km and 12 km altitude in the tropical eastern Pacific. The correlation coefficients are −0.79 (−0.84) in the MTT simulation, and −0.76 (−0.83) in the HTT simulation at 3 (12) km altitude. The ozone anomaly in the regions follows the Niño3.4 index during the positive phase of ENSO. The difference between the anomaly and the index stands out during the negative phase of ENSO. The month-to-month variation also contributes to the difference.

Figure 4a presents the partial regression coefficient of ozone observed by the MLS/TES instruments with respect to the Niño3.4 index averaged in the tropics (15°S–15°N). The MLS/TES observation shows a positive anomaly over Indonesia and the Indian Ocean. Local peaks of the anomaly are located at 80°E and at 14 km altitude (up to 5 ppbv/K), and at 100°E at altitudes between 5 and 10 km (up to 3 ppbv/K). A negative anomaly of about 2 ppbv/K is found in the middle troposphere over the central and eastern Pacific. The anomaly reaches 10 ppbv/K near the tropopause. The regression coefficient of ozone in the MTT simulation shows a similar spatial pattern to that in the MLS/TES observation (Figure 4b). However, the MTT simulation underestimates the magnitude of the observed anomalies. The HTT simulation generally shows a spatial pattern of the anomalies similar to that in the MTT simulation, although the HTT simulation partly improves the underestimation in the central and eastern Pacific. However, the anomaly over Indonesia and

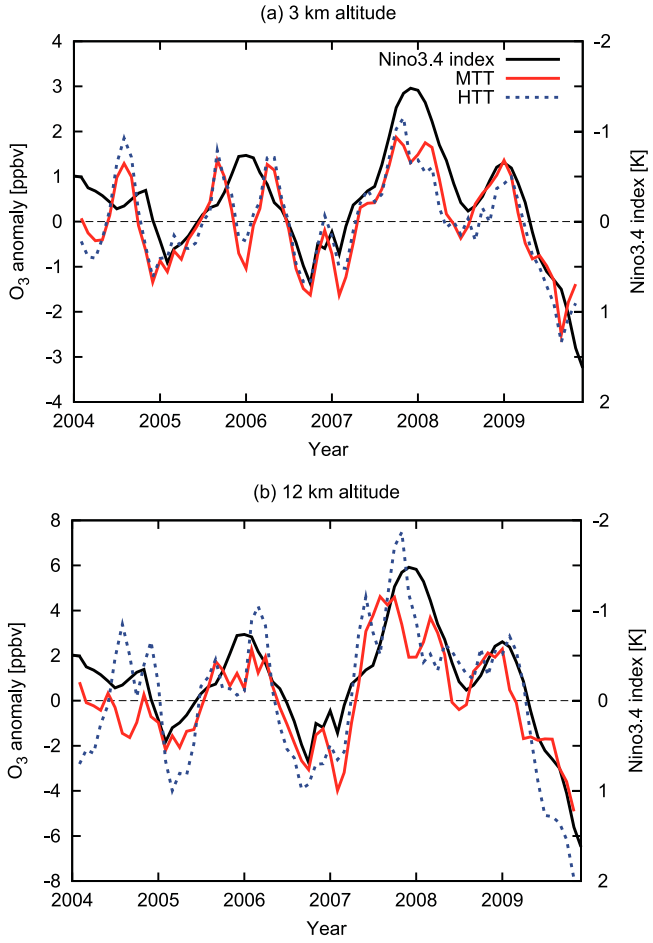

Figure 3. Three month running mean of the Niño3.4 index (*K*) and ozone anomaly (ppbv) in the MTT simulation and the HTT simulation averaged in the tropical eastern Pacific (180°–240°E, 15°S–15°N). (a) At 3 km altitude and (b) at 12 km altitude. The black line shows the Niño3.4 index, the red line is the anomaly in the MTT simulation, and the blue line is the anomaly in the HTT simulation. The left and right *y* axes, respectively, show the anomaly of ozone and the Niño3.4 index. The right *y* axis is reversed.

the Indian Ocean is underestimated in the MTT and HTT simulations (about 1 ppbv/K) because the monthly mean emission from biomass burning in 2000 was used in the simulations during 2004–2009. In the tropical lower stratosphere, the observed and the modeled variation in ozone show a negative anomaly of approximately 20 ppbv/K. The spatial pattern of the variation in tropospheric ozone in our model is similar to that in HadAM3-STOCHEM [*Doherty et al.*, 2006] and Goddard Earth Observing System Chemistry-Climate Model (GEOSCCM) [*Oman et al.*, 2013], despite their different simulation periods. The simulation periods are 6 years (2004–2009) in this study, 23 years (1980–2002) in *Doherty et al.* [2006], and 25 years (1985–2009) in [*Oman et al.* 2013].

The difference of the anomalies between the MTT and the HTT simulations is mainly attributable to the increased horizontal resolution of the representation of atmospheric circulation and advection because the simulations prescribed the same chemical production and loss rate of O_x. One reason for the difference is the different response of the Walker circulation to the observed SST variation. We calculate the sensitivity of the simulated Walker circulation to the observed SST variation using the Southern Oscillation Index (SOI) as a proxy of the Walker circulation and compare it with the sensitivity of the SOI obtained from NOAA CPC (http://www.cpc.ncep.noaa.gov/data/indices/). We defined the sensitivity as a linear regression coefficient of the SOI with respect to the Niño3.4 index. The sensitivities are $-0.53 \pm 0.29\mathrm{K}^{-1}$ in the MTT simulation, $-0.72 \pm 0.23\mathrm{K}^{-1}$ in the HTT simulation, and $-0.88 \pm 0.22\mathrm{K}^{-1}$ in the observation. The range of the sensitivities is a two-sided 95% confidence interval. These sensitivities indicate that the Walker circulation in the HTT simulation is more sensitive to the observed SST variation than that in the MTT simulation. The sensitivity

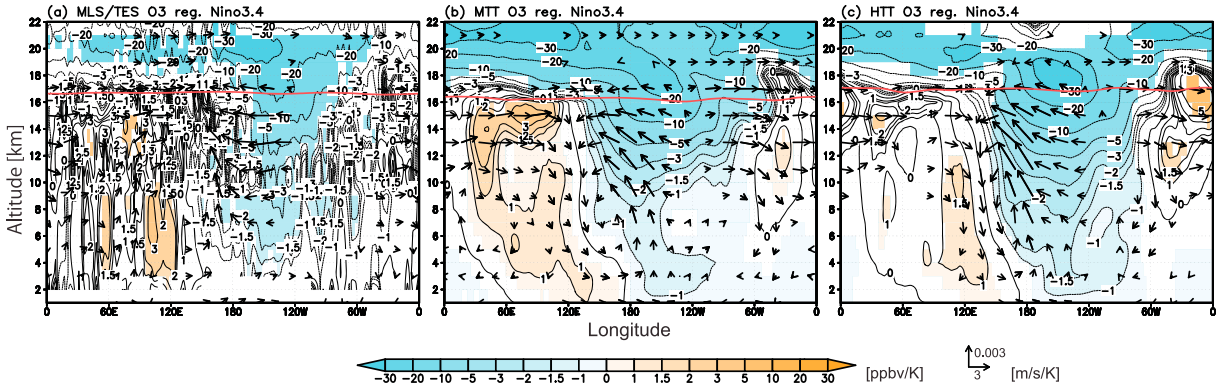

Figure 4. Regression and partial regression coefficients of ozone (ppbv/K) and wind field (m/s/K) with respect to the Niño3.4 index averaged in the tropics (15°S–15°N) during 2004–2009. The shaded regions show a significant ozone variation at a 95% confidence level. Arrows indicate a wind field variation at a 95% confidence level: (a) the partial regression coefficient in the MLS/TES observation (ozone) and the ERA-Interim (wind), (b) the regression coefficient in the MTT simulation, and (c) the partial regression coefficient in the HTT simulation. The vertical component of wind is multiplied by 1000. The red line is the tropopause height, which is determined from temperature lapse rate using the WMO definition [*WMO*, 1957]. The tropopause height in the left panel is calculated from the ERA-Interim.

in the MTT simulation is out of the range of the observed sensitivity, although that in the HTT simulation is within the range of the observed sensitivity.

In the eastern Pacific, positive anomalies in the MLS/TES observation and the simulations are apparent at 12–20 km altitudes over the subtropics and the midlatitudes (Figure 5). The positive anomalies in the MTT simulation (about 10 ppbv/K) are weaker than those in the MLS/TES observation (about 50 ppbv/K), especially in the Northern Hemisphere, although the anomalies in the HTT simulation are comparable to those in the MLS/TES observation. The simulated positive anomalies extend to the low to middle troposphere over the subtropics (0.5–1 ppbv/K). The simulated anomalies are in agreement with the observed anomalies. These anomalies are slightly weaker than those in GEOSCCM (2–3 ppbv/K in the low to middle troposphere and 10–15 ppbv/K near the tropopause shown in *Oman et al.* [2013, Figure 4]). The anomalies can result from enhanced transport of Asian pollution and increased stratosphere-troposphere exchange of ozone during El Niño [*Langford et al.*, 1998; *Hsu et al.*, 2005; *Zeng and Pyle*, 2005; *Koumoutsaris et al.*, 2008; *Voulgarakis et al.*, 2011], reflecting the intensified subtropical jet, and the enhanced local Hadley circulation, and the accelerated Brewer-Dobson circulation [*Shapiro et al.*, 2001; *Wang*, 2002; *Calvo et al.*, 2010]. The enhanced meridional circulation is also shown in Figure 5 with arrows. A negative anomaly is also found in the tropics in the MLS/TES observation and the simulations. As with *Oman et al.* [2013], the modeled negative anomaly is narrower in latitude than the observed anomaly in the tropical troposphere. The HTT

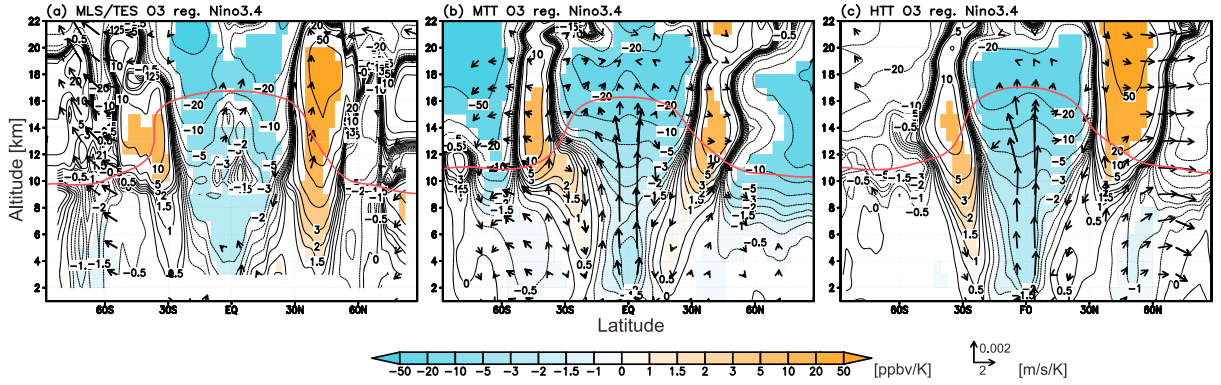

Figure 5. Regression and partial regression coefficients of ozone (ppbv/K) and wind field (m/s/K) with respect to the Niño3.4 index averaged in the eastern Pacific (180°–230°E) during 2004–2009. The shaded regions show a significant ozone variation at a 95% confidence level. Arrows indicate a wind field variation at a 95% confidence level: (a) the partial regression coefficient in the MLS/TES observation (ozone) and the ERA-Interim (wind), (b) the regression coefficient in the MTT simulation, and (c) the partial regression coefficient in the HTT simulation. The vertical component of wind is multiplied by 1000. The red line shows the tropopause height. The tropopause height in the left panel is calculated from the ERA-Interim.

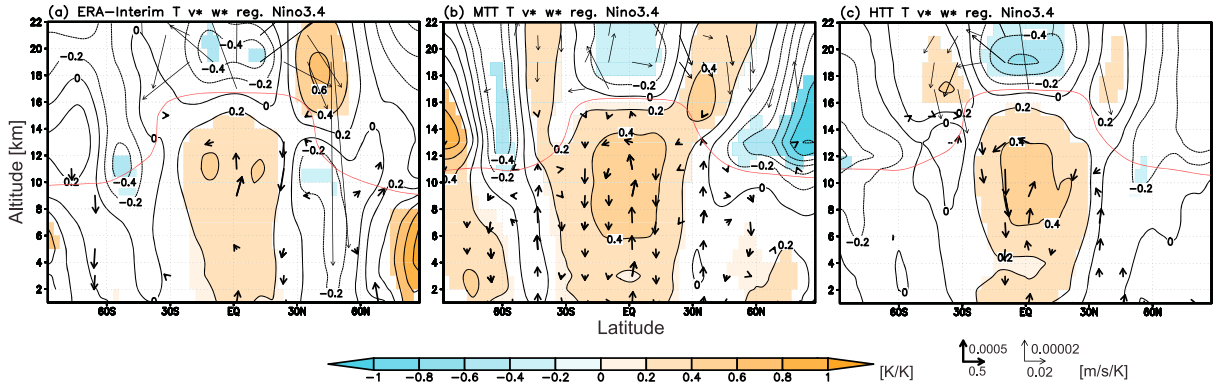

Figure 6. Regression and partial regression coefficients of zonal mean temperature (K/K) and residual circulation (m/s/K) with respect to the Niño3.4 index during 2004–2009. The shaded regions show a significant temperature variation at a 95% confidence level. Arrows indicate a wind field variation at a 95% confidence level: (a, c) the partial regression coefficient in the ERA-Interim and the HTT simulation, respectively; (b) the regression coefficient in the MTT simulation. The vertical component of residual circulation is multiplied by 1000. The scale of the thin arrow is 25 times larger than that of the thick arrow. The red line is the tropopause height. The tropopause height in the left panel is calculated from the ERA-Interim.

simulation improves the tropical negative anomaly in the middle troposphere compared to that in the MTT simulation.

We also investigate the zonal mean response of temperature and ozone to ENSO. Figure 6 shows the temperature regression and partial regression coefficients with respect to the Niño3.4 index. In the tropical troposphere, the ERA-Interim data, the MTT simulation, and the HTT simulation show a positive anomaly, although the simulations overestimate the anomaly in the ERA-Interim. In contrast, a negative anomaly of 0.4 K/K is found in the tropical lower stratosphere in the ERA-Interim. The simulations also show the negative anomaly of 0.2 K/K in the MTT simulation and 0.6 K/K in the HTT simulation. Over 30°–60°N and S, positive anomalies are found in the lower stratosphere. The model underestimates the positive anomaly of 0.6 K/K in the ERA-Interim in the Northern Hemisphere. The difference between the ERA-Interim and the simulations is attributable to the weak anomalous descent in the lower stratosphere of the northern midlatitude. The spatial pattern of the anomalies of temperature in this study is similar to that in SAGE observation, ozonesonde observation, and the simulation with WACCM [*Randel et al.*, 2009; *Randel and Thompson*, 2011].

Regarding zonal mean ozone, the MLS/TES observation and the simulations show a negative anomaly in the tropical lower stratosphere, and positive anomalies in the midlatitude lower stratosphere (Figure 7). In the tropical lower stratosphere, the negative anomaly in the MTT and HTT simulations is comparable to the observed one (20–30 ppbv/K). However, the simulated positive anomaly above 18 km altitude over 30°–60°N (about 5 ppbv/K in the MTT simulation and 10 ppbv/K in the HTT simulation) underestimates the observed one (about 50 ppbv/K). At 12–18 km altitude over 30°–60°S, the HTT simulation reproduces

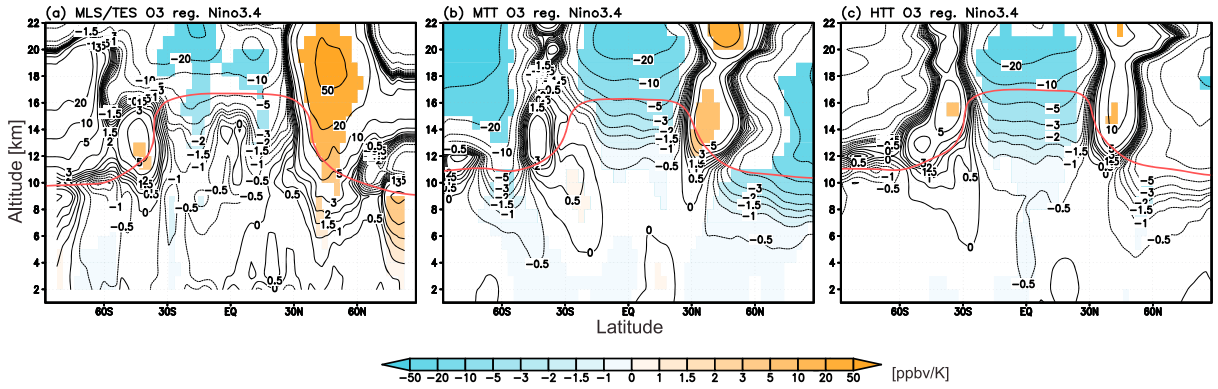

Figure 7. Regression and partial regression coefficients of zonal mean ozone (ppbv/K) with respect to the Niño3.4 index during 2004–2009. The shaded regions show a significant ozone variation at a 95% confidence level: (a, c) the partial regression coefficients in the MLS/TES observation and the HTT simulation, respectively; (b) the regression coefficient in the MTT simulation. The red line shows the tropopause height. The tropopause height in the left panel is calculated from the ERA-Interim.

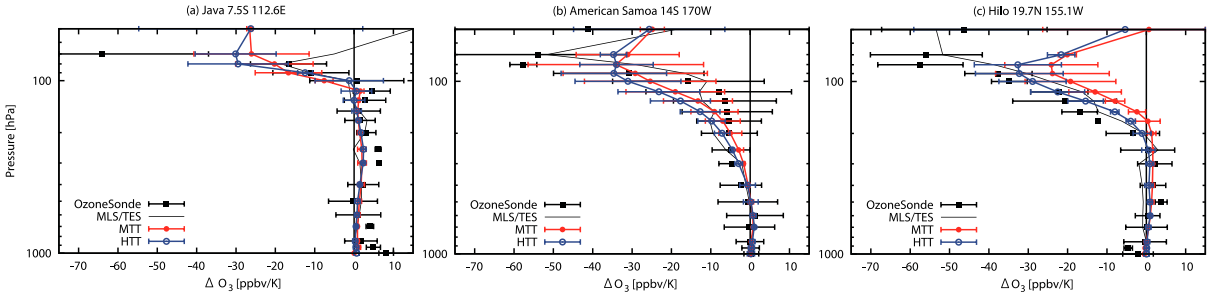

Figure 8. Regression and partial regression coefficients of ozone with respect to the Niño3.4 index (ppbv/K) at (a) Java, (b) Samoa, and (c) Hilo during 2004–2009. The black squares and line, respectively, stand for the partial regression in the ozonesonde observation and the MLS/TES observation. The red line shows the regression in the MTT simulation. The blue one denotes the partial regression in the HTT simulation. The error bar represents a range of a two-sided 95% confidence interval.

the positive anomaly of approximately 5 ppbv/K derived from MLS and TES, although the MTT simulation underestimates it slightly. *Randel et al.* [2009] and *Randel and Thompson* [2011] also analyzed SAGE and ozonesonde observations and the simulation with WACCM. Results of this study show the regression coefficient of −2.5–3% per standardized Niño3.4 index in the tropical lower stratosphere and the regression coefficients of 0.6–1.2% per standardized Niño3.4 index in the midlatitude lower stratosphere. However, the regressions in the MTT and HTT simulations are weaker than those in *Randel et al.* [2009] and *Randel and Thompson* [2011].

Additionally, we compare the ENSO-related variation in the MLS/TES observation and the simulations with that in the ozonesonde observation during 2004–2009 in the tropical Pacific. This evaluation is similar to that in *Oman et al.* [2011], which used the observation in the two western region SHADOZ locations (Java and Kuala Lumpur) and the three eastern region SHADOZ locations (Samoa, Hilo, and San Cristobal) for 1998–2009. At Java, the simulations, the MLS/TES observation, and the ozonesonde observation show ozone increases in the troposphere (Figure 8a). However, the simulations slightly underestimate the increase observed by the ozonesonde observation. At Samoa, the observed and the simulated ozone are decreased, although the simulated ozone underestimates the observed one in the middle troposphere (Figure 8b). At Hilo, the simulations and the ozonesonde observation show a positive anomaly in the middle troposphere and a negative anomaly in the upper troposphere (Figure 8c). The HTT simulation partly improves the underestimation of the negative anomaly in the upper troposphere. In the tropical lower stratosphere, a negative anomaly of about 40 ppbv/K is observed at all stations. The simulations tend to underestimate the observed negative anomaly (10–34 ppbv/K). The vertical profiles of the regression coefficient with respect to the Niño3.4 index in this study are similar to that in *Oman et al.* [2011].

Table 3. Vertical Mass (Ozone in Parentheses) Flux at 100 hPa[a]

	90°S–20°S	20°S–25°N	25°N–90°N
	ENSO-Related Variation		
ERA-Interim	−17.6 ± 6.0	37.0 ± 10.7	−19.3 ± 5.3
	(−16.7 ± 4.3)	(3.1 ± 5.2)	(−24.8 ± 17.2)
MTT	−3.2 ± 4.6	14.6 ± 3.9	−11.4 ± 4.7
	(0.9 ± 14.2)	(−0.7 ± 2.5)	(−11.2 ± 4.3)
HTT	−13.4 ± 1.1	17.4 ± 1.6	−4.0 ± 11.6
	(−9.5 ± 10.0)	(−2.2 ± 2.6)	(−1.2 ± 39.2)
	Change Between the 2000s and 2100s		
MTT	−2.98 ± 0.76	6.24 ± 0.92	−3.30 ± 0.75
	(−5.19 ± 1.50)	(−0.21 ± 0.36)	(−1.93 ± 1.99)
HTT	−5.19 ± 0.59	10.33 ± 0.96	−5.14 ± 0.63
	(−9.11 ± 1.34)	(0.07 ± 0.43)	(−5.22 ± 2.00)

[a]The positive sign denotes upward flux. The top four rows are regression or partial regression coefficients with respect to the Niño3.4 index, and the bottom four rows are the future change between the 2000s and 2100s. The unit of mass flux is 10^6 Tg/yr/K for the ENSO-related variation and is 10^6 Tg/yr/decade for the future change between the 2000s and 2100s. The unit of ozone flux is Tg/yr/K for the ENSO-related variation and is Tg/yr/decade for the future change. The range is defined as a two-sided 95% confidence interval for the ENSO-related variation and is defined as a root-sum-square value of the standard deviation in simulations for the future change.

Table 3 shows ENSO-related variation in the vertical mass flux at 100 hPa. During the positive phase of ENSO (El Niño), increases in upward and downward mass fluxes are seen, respectively, in the tropics and the extratropics. The change in the simulated fluxes is, however, underestimated compared to the fluxes in the ERA-Interim. The MTT simulation presents the flux change stronger than that in the HTT simulation

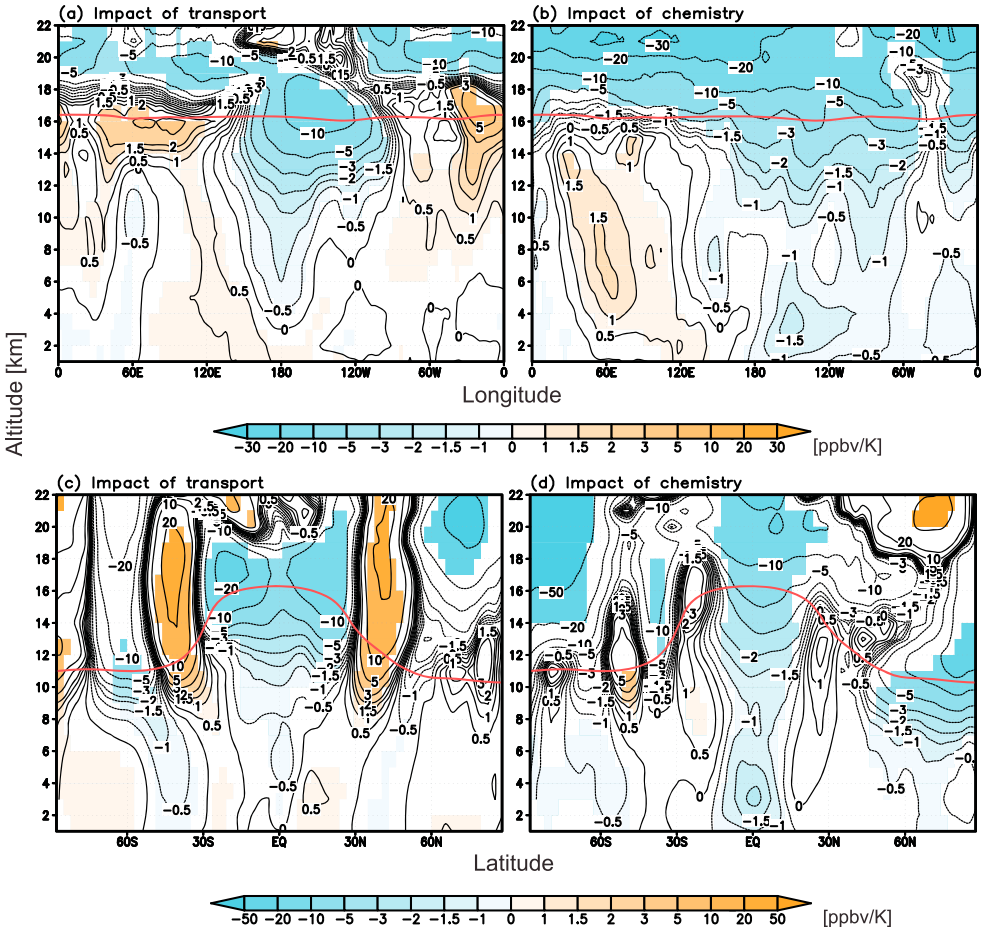

Figure 9. Impacts of (a, c) transport and (b, d) chemistry on the regression coefficients of ozone (ppbv/K) with respect to the Niño3.4 index estimated from the MTT simulation and the MTT-fCHEM simulation during 2004–2009. Figures 9a and 9b and Figures 9c and 9d, respectively, show the average in the tropics (15°S–15°N) and the eastern Pacific (180°–230°E). The shaded regions show a significant ozone variation at a 95% confidence level. The red line is the tropopause height.

in the northern extratropics, although the difference is within the range of the two-sided 95% confidence interval. In the southern extratropics, the MTT simulation shows the flux change weaker than that in the HTT simulation, and the difference exceeds the range. In the tropics, the HTT simulation exhibits the change in the flux slightly larger than that in the MTT simulation. We estimate the vertical ozone flux at 100 hPa from a wind field of the ERA-Interim and an ozone field of the MLS/TES data. The flux indicates increases in upward and downward ozone fluxes, respectively, in the tropics and the extratropics (Table 3). The change in the ozone fluxes in the simulations is weaker than the change estimated from the ERA-Interim and the MLS/TES data in all latitude bands.

We also quantify the individual impacts of transport and chemical processes on the ozone variation. The MTT simulation accommodates year-to-year variation of both the transport field (wind field) and chemical field (P and β of O_x), although the MTT-fCHEM simulation allows only the transport field to vary among years. The impact of transport is defined as a regression coefficient of ozone in the MTT-fCHEM simulation with respect to the Niño3.4 index. We also define the impact of chemistry as a regression coefficient of ozone difference between the MTT simulation and the MTT-fCHEM simulation with respect to the Niño3.4 index. The simulations present that transport and chemistry have comparable impacts on the ozone variation in the tropics (Figures 9a and 9b). However, the impact of chemistry is dominant in the lower troposphere over the central and eastern Pacific. Our simulations show that the impact of chemistry is greater than that shown in *Sekiya and Sudo* [2012, Figure 6] over the Indian Ocean. This difference reflects an increase in the production rate of O_x over Africa in the FC simulation, in which a regression coefficient of lightning NO_x production with respect to the Niño3.4 index is positive (7.3 kg N/m^2/s/K) over Africa.

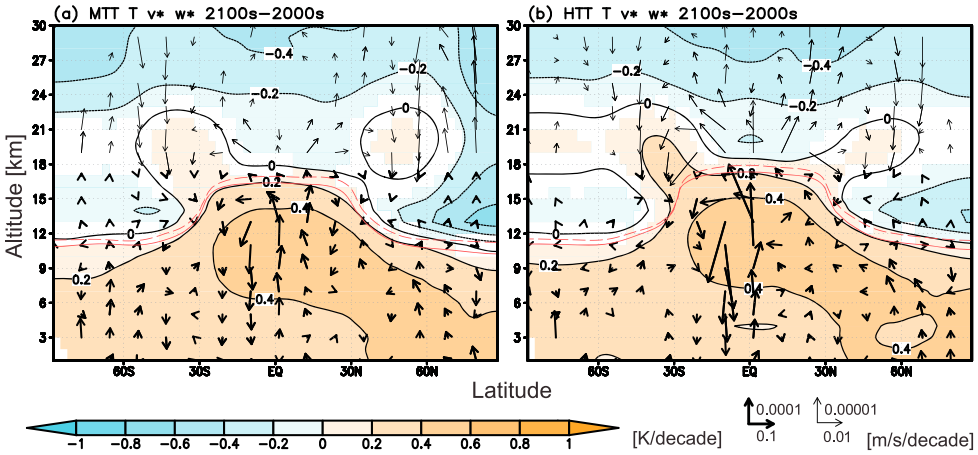

Figure 10. Changes in annual and zonal mean temperature (K/decade) and residual circulation (m/s/decade) between the 2000s and 2100s. The shaded regions show significant temperature changes at a 98% confidence level. The arrows indicate a wind field change at a 98% confidence level: (a) the MTT simulation and (b) the HTT simulation. The vertical component of residual circulation is multiplied by 1000. The scale of the thin arrow is 10 times larger than that of the thick arrow. The solid red line is the tropopause height in the simulations for the 2000s, and the dashed red line is the tropopause height in the simulations for the 2100s.

In the subtropics over the eastern Pacific, transport and chemistry play significant roles in most regions. Nevertheless, the impacts of transport are dominant in the midlatitude lower stratosphere over the eastern Pacific (Figures 9c and 9d). The model also calculates separate tracers for O_3 produced in the stratosphere ($p > 100$ hPa) and the troposphere ($p < 100$ hPa). These indicate that ozone from the stratosphere and the troposphere, respectively, contribute to the ozone increase because of transport in the upper troposphere and lower stratosphere. In the lower troposphere, ozone from the troposphere dominates the ozone increase. These results also suggest that the ozone increase in the subtropics is caused not only by the intensified stratosphere-troposphere ozone exchange but also by the variation in tropospheric transport. For example, the export of Asian pollution to the Pacific is enhanced during El Niño, resulting from intensification and a southward shift of the northern subtropical jet over the eastern Pacific [*Koumoutsaris et al.*, 2008].

5. Future Changes

We performed future projections of climate and ozone and investigated the future changes. The sensitivity of the change to the horizontal resolution is also assessed by comparing the projection with two horizontal resolutions (about 300 km and 120 km). We used the results obtained for the last 5 years for each period. Figure 10 portrays the change in annual and zonal mean temperature between the 2000s and 2100s. The MTT simulation shows warming of 4 K in the troposphere and cooling of 4 K in the stratosphere (Figure 10a). The HTT simulation exhibits warming similar to that in the MTT simulation in the troposphere. Moreover, the HTT simulation predicts slightly stronger cooling in the tropical lower stratosphere, weaker cooling in the high latitudes in the lower stratosphere, and stronger warming in the subtropical lower stratosphere (Figure 10b).

The model predicts an increase in the global stratospheric ozone burden by 0.24 ± 0.01%/decade in the MTT simulation and by 0.29±0.01%/decade in the HTT simulation. We regard an uncertainty range of the change as a root-sum-square value of the standard deviation in the simulations for the 2000s and the 2100s. The predicted changes in annual and zonal mean ozone between the 2000s and 2100s show a decrease by 20 ppbv/decade in the tropical lower stratosphere, as well as an increase by 20 ppbv/decade in the extratropical lower stratosphere (Figure 11). An uncertainty range of the change is smaller than the change (30% of the change) in most of the region where the change is confident at the 98% level (shaded region). The difference of the changes in stratospheric ozone in the MTT and HTT simulations is within the range of the changes, except in the lower stratosphere over the northern high latitudes, where the difference reaches 18 ppbv/decade (about 2 times larger increase) at 23 km altitude. The global annual mean ozone change at 50 hPa is −2.8 ppbv/decade in the MTT simulation and −1.4 ppbv/decade in the HTT simulation, which

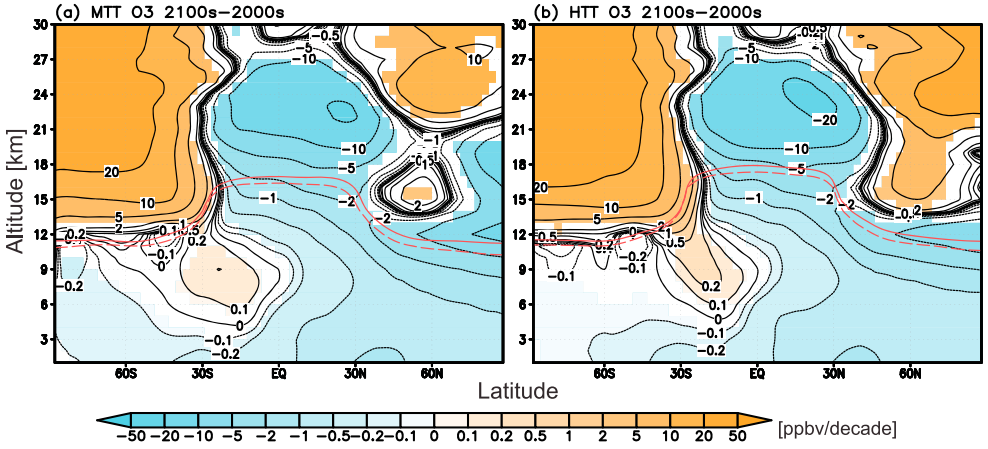

Figure 11. Changes in annual and zonal mean ozone (ppbv/decade) between the 2000s and 2100s. The shaded regions show significant ozone changes at a 98% confidence level: (a) the MTT simulation; (b) the HTT simulation. The solid red line is the tropopause height in the simulations for the 2000s, and the dashed red line is the tropopause height in the simulations for the 2100s.

are smaller and opposite changes compared to the multimodel mean of CMIP5 and CCMVal-2 models [*Eyring et al.*, 2013a]. Particularly, we must interpret the change in the lower stratosphere over the northern middle to high latitudes with some caution because our model simulates a decrease in ozone at 50 hPa over there, in contradiction to the result of CMIP5 models.

The global tropospheric ozone burden is reduced between the 2000s and 2100s by 0.82 $\pm$ 0.04%/decade in the MTT simulation and by 0.76 $\pm$ 0.04%/decade in the HTT simulation. A reduction of the tropospheric ozone concentration is typically 0.8 ppbv/decade in the free troposphere over the northern midlatitudes (Figure 11). The simulated tropospheric ozone is increased slightly in the upper troposphere over the southern subtropics (typically $\leq$ 0.2 ppbv/decade). An uncertainty range of the change is smaller than the change (30% of the change) in most of the region where the change is confident at the 98% level (shaded region). The difference of the tropospheric ozone change between the MTT and HTT simulations is less than 0.1 ppbv/decade in the middle and lower troposphere and is comparable to the range of the change in tropospheric ozone. In comparison with the time-slice simulations for the 2000s and the 2100s along with RCP6 scenario in *Young et al.* [2013], the reduction of the global tropospheric ozone burden in this study is similar to that simulated by the ACCMIP models (0.9%/decade). The change in tropospheric ozone in this study also shows a similar value to that in the ACCMIP models (0.5–1 ppbv/decade) in the free troposphere over the northern midlatitudes. In the Southern Hemisphere, our simulations show no increase in tropospheric ozone, as shown in the mean of the ACCMIP models. However, our model predicts the reduction of the global tropospheric ozone burden larger than that (−0.15%/decade) in *Kawase et al.* [2011].

The differences of temperature and ozone between the MTT and HTT simulations are at least partially attributable to a difference in the strengthening of the Brewer-Dobson circulation (BDC). The HTT simulation shows an acceleration of BDC stronger than that in the MTT simulation (arrows in Figure 10). At 100 hPa, the vertical mass flux is strengthened by 20% in the MTT simulation and by 25% in the HTT simulation in the 2100s compared to the 2000s (Table 3). The acceleration of BDC results in an increase of ozone influx from the stratosphere to the troposphere. We also examine the vertical ozone flux at 100 hPa instead of STE ozone flux (Table 3). The upward ozone flux is not altered significantly in the tropics because the ozone decrease and the enhanced upwelling cancel each other out at 100 hPa. The downward ozone fluxes in the extratropics of Northern and Southern Hemispheres are increased in the MTT simulation (1.93 and 5.19 Tg/yr/decade, respectively). The HTT simulation predicts that the downward fluxes in the northern and southern extratropics are, respectively, 5.22 and 9.11 Tg/yr/decade, which are about 2 times larger than those in the MTT simulation.

The future ozone change results from changes in ozone transport (e.g., changes due to atmospheric circulation, convection, and vertical diffusion) and changes in chemical ozone production and loss (e.g., changes due to temperature, water vapor, emissions of ozone precursors and ODSs). This study regards bringing air mass to a region with lower or higher water vapor as an impact of transport processes. To ascertain the

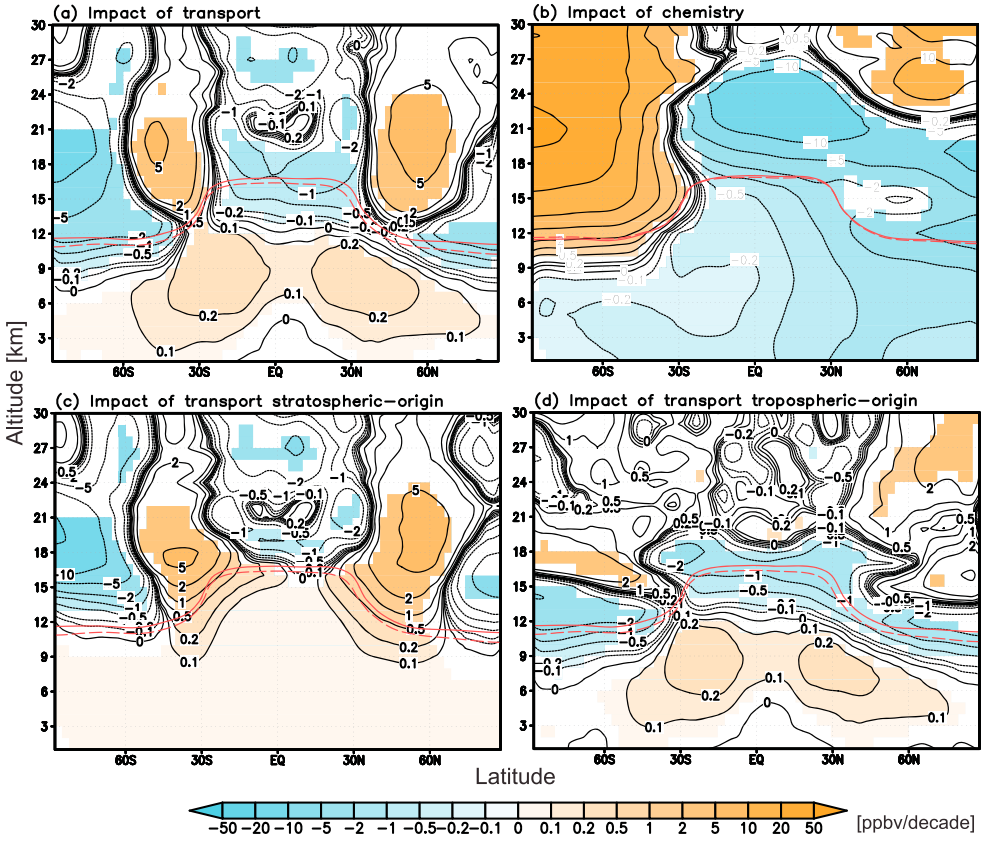

Figure 12. Impacts of (a) transport and (b) chemistry on the annual and zonal mean changes in ozone (ppbv/decade) between the 2000s and 2100s, as estimated from the MTT simulation and the MTT-fCHEM simulation. Impact of transport on future changes in separate O_3 tracers produced in (c) the stratosphere and (d) the troposphere (ppbv/decade) in the MTT-fCHEM simulation. The shaded regions show significant ozone changes at a 98% confidence level. In Figure 12b the solid red line and the dashed red line, respectively, show the tropopause height in the MTT-fCHEM simulation and in the MTT simulation for the 2100s. In the other panels, the solid red line and the dashed red line, respectively, denote the tropopause in the MTT simulation for the 2000s and in the MTT-fCHEM simulation.

processes determining the future change in ozone, we investigate the individual impacts of transport and chemistry on the future ozone change. The MTT simulation for the 2000s and the 2100s calculates ozone with the transport field (wind field) and the chemical field (P and β of O_x) for the corresponding period. The MTT-fCHEM simulation calculates ozone with the transport field for the 2100s and the chemical field for the 2000s. We define the impact of transport as the difference between the MTT-fCHEM simulation and the MTT simulation for the 2000s. Moreover, we define the impact of chemistry as the difference between the MTT simulation for the 2100s and the MTT-fCHEM simulation. Figures 12a and 12b, respectively, depict the ozone change between the 2000s and 2100s attributable to transport and chemistry. The change in ozone is driven mainly by chemistry in the stratosphere. The decrease in ODSs dominates the ozone increase attributable to chemistry in the extratropical lower stratosphere of the Southern Hemisphere. In the tropical lower stratosphere and the extratropical lower stratosphere of the Northern Hemisphere, the decrease in ozone attributable to chemistry is caused by a decrease in the production of ozone, which exceeds a decrease in the loss of ozone. The decrease in production is related to a decrease in the actinic flux through an overhead ozone increase. The decrease in actinic flux also leads to a decrease in OH through the reaction of $H_2O + O(^1D)$, although an effect of increased water vapor compensates an effect of decreased $O(^1D)$ in the FC simulation.

In the troposphere, chemistry processes cause a reduction of the global tropospheric ozone burden by 1.07%/decade, reflecting the emission reductions of tropospheric ozone precursors and climate change (Figure 12b). Transport processes increase the global burden of tropospheric ozone by 0.25%/decade, corresponding to 23% of the decrease in the global tropospheric ozone burden attributable to chemistry

(Figure 12a). The model also calculates separate tracers for O_3 produced in the stratosphere ($p > 100$ hPa) and the troposphere ($p < 100$ hPa). Figures 12c and 12d suggest that the increase in the global tropospheric ozone burden attributable to transport is contributed by ozone of both the tropospheric origin (57%) and the stratospheric origin (43%).

6. Summary and Conclusion

This study investigates ozone changes and the individual impacts of transport and chemistry on those changes. We specifically examined (1) the variation related to El Niño Southern Oscillation (ENSO), which is a dominant mode of the interannual variation of the tropospheric ozone, and (2) the long-term change between the 2000s and 2100s. Additionally, we conducted simulations at two horizontal resolutions (about 300 km and 120 km) to test a sensitivity of ozone changes to the increased horizontal resolution of the representation of atmospheric circulation and advection. However, we do not consider any aspect of the nonlinearity of ozone chemistry sensitivity to horizontal resolution. Our model captures general features of the observed ozone climatology, although the simulated ozone is high biased in the lower stratosphere and is low biased in the troposphere. These biases in the simulation of two resolutions are similar.

To evaluate our CCM, this study examined the ENSO-related variation in tropospheric and lower stratospheric ozone in the simulations of medium resolution and high resolution forced by the observed SST variability. The medium-resolution and high-resolution simulations show an increase in tropospheric ozone (1 ppbv/K) over Indonesia, and a decrease (2–10 ppbv/K) in the tropical eastern Pacific. The results generally agree with the variation observed by the MLS/TES instruments. In the midlatitude lower stratosphere over the eastern Pacific, increases by 10 ppbv/K and by 50 ppbv/K are also found, respectively, in the medium-resolution and high-resolution simulations. The simulated increase in the high-resolution simulation agrees with the observed one better. In the other regions, no great difference is found between the two simulations.

To investigate the processes determining the ENSO-related variation of ozone, we quantified the individual impacts of transport and chemistry using a sensitivity simulation fixed to the average chemical field for 2004–2009. The simulation shows that transport and chemistry play important roles in the ozone variation in most regions. However, chemistry strongly affects the ozone decrease in the tropical lower troposphere over the eastern Pacific. Transport processes dominate the ozone increases in the midlatitude lower stratosphere over the eastern Pacific. Transport of ozone of both the stratospheric origin and the tropospheric origin contribute to the upper tropospheric ozone increase, although the ozone increase results from ozone of the tropospheric origin in the lower and middle troposphere.

We also investigated the future change in stratospheric and tropospheric ozone between the 2000s and 2100s under the RCP6 scenario in the time-slice simulations of the two resolutions. The model predicts an increase in the global stratospheric ozone burden by 0.24 $\pm$ 0.01%/decade in the medium-resolution simulation and by 0.29 $\pm$ 0.01%/decade in the high-resolution simulation. The predicted changes in annual and zonal mean ozone show a decrease by 20 ppbv/decade in the tropical lower stratosphere, and an increase by 20 ppbv/decade in the extratropical lower stratosphere. However, the medium-resolution simulation predicts a decrease in ozone in the lower stratosphere over the northern middle to high latitudes (5–10 ppbv/decade). This result is opposite to that of CMIP5 models shown in *Eyring et al.* [2013a]. It is necessary to interpret the ozone change there with particular caution because our model simulates the decrease in ozone there in contradiction to the results obtained from CMIP5 models. The global tropospheric ozone burden is reduced by 0.82 $\pm$ 0.04%/decade in the medium-resolution simulation and by 0.76 $\pm$ 0.04%/decade in the high-resolution simulation. A reduction of tropospheric ozone concentration is typically 0.8 ppbv/decade in the free troposphere over the northern midlatitudes. The changes in the global burden of stratospheric and tropospheric ozone in the medium-resolution and high-resolution simulations are different, although the differences are comparable to the uncertainty range of the changes.

To elucidate the processes determining the future change in ozone, we investigated the individual impacts of transport and chemistry on the ozone change using a sensitivity simulation with the 2100s transport field and the 2000s chemical field. The change in the global stratospheric ozone burden is controlled by chemical processes. Chemical processes also reduce the global burden of tropospheric ozone by 1.07%/decade. However, transport processes increase the burden by 0.25%/decade. The increase attributable to transport is contributed to by ozone of both the stratospheric origin and the tropospheric origin. This fact suggests not only that the increased influx of stratospheric ozone causes the increase in the global tropospheric ozone

burden as shown in the previous studies [e.g., *Collins et al.*, 2003; *Sudo et al.*, 2003; *Zeng and Pyle*, 2003] but also that the future change in tropospheric circulation raises the global tropospheric ozone burden.

Our results are obtained from one model. To confirm the robustness of our result, it is necessary to compare the results of other models such as the Chemistry Climate Model Initiative models [*Eyring et al.*, 2013b]. We also examined the respective impacts of transport and chemical processes on the future change in stratospheric and tropospheric ozone. However, the result must be interpreted with caution because they are estimated from the simulations conducted only with the medium horizontal resolution. In addition, a detailed investigation of the future ozone change attributable to chemical processes is not performed. Additional simulations and analyses must be done to assess the impacts of tropospheric ozone precursor emissions, ODS emissions, and climate change.

Acknowledgments

This research was supported by the Global Environment Research Fund (S-7) of the Ministry of the Environment (MOE), Japan, and the Research Program on Climate Change Adaptation (RECCA) by the Ministry of Education, Culture, Sports, Science and Technology (MEXT), Japan. We are grateful to ECMWF for providing ERA-Interim reanalysis. MLS and TES data were obtained from Earth Observing System Data and Information System (EOSDIS). We thank NCAR Earth System Laboratory Atmospheric Chemistry Division (http://www.acd.ucar.edu/gctm/download.shtml) for providing the ozonesonde climatology data. The ozonesonde data at Java, Samoa, and Hilo during 2004–2009 were obtained from SHADOZ (http://croc.gsfc.nasa.gov/shadoz/). Simulations were performed using the NIES supercomputer system. Finally, we thank three anonymous reviewers for their helpful comments.

References

Akiyoshi, H., T. Sugita, H. Kanzawa, and N. Kawamoto (2004), Ozone perturbations in the Arctic summer lower stratosphere as a reflection of NO_X chemistry and planetary scale wave activity, *J. Geophys. Res.*, *109*, D03304, doi:10.1029/2003JD003632.

Allen, R. J., S. C. Sherwood, J. R. Norris, and C. S. Zender (2012), Recent Northern Hemisphere tropical expansion primarily driven by black carbon and tropospheric ozone, *Nature*, *485*(7398), 350–354.

Brasseur, G. P., M. Schultz, C. Granier, M. Saunois, T. Diehl, M. Botzet, E. Roeckner, and S. Walters (2006), Impact of climate change on the future chemical composition of the global troposphere, *J. Clim.*, *19*(16), 3932–3951, doi:10.1175/JCLI3832.1.

Calvo, N., R. R. Garcia, W. J. Randel, and D. R. Marsh (2010), Dynamical mechanism for the increase in tropical upwelling in the lowermost tropical stratosphere during warm enso events, *J. Atmos. Sci.*, *67*(7), 2331–2340, doi:10.1175/2010JAS3433.1.

Chandra, S., J. R. Ziemke, W. Min, and W. G. Read (1998), Effects of 1997–1998 El Niño on tropospheric ozone and water vapor, *Geophys. Res. Lett.*, *25*(20), 3867–3870, doi:10.1029/98GL02695.

Chandra, S., J. R. Ziemke, P. K. Bhartia, and R. V. Martin (2002), Tropical tropospheric ozone: Implications for dynamics and biomass burning, *J. Geophys. Res.*, *107*(D14), 4188, doi:10.1029/2001JD000447.

Chandra, S., J. R. Ziemke, B. N. Duncan, T. L. Diehl, N. J. Livesey, and L. Froidevaux (2009), Effects of the 2006 El Niño on tropospheric ozone and carbon monoxide: Implications for dynamics and biomass burning, *Atmos. Chem. Phys.*, *9*(13), 4239–4249, doi:10.5194/acp-9-4239-2009.

Colella, P., and P. R. Woodward (1984), The Piecewise Parabolic Method (PPM) for gas-dynamical simulations, *J. Comput. Phys.*, *54*(1), 174–201, doi:10.1016/0021-9991(84)90143-8.

Collins, W. J., R. G. Derwent, B. Garnier, C. E. Johnson, M. G. Sanderson, and D. S. Stevenson (2003), Effect of stratosphere-troposphere exchange on the future tropospheric ozone trend, *J. Geophys. Res.*, *108*(D12), 8528, doi:10.1029/2002JD002617.

Doherty, R. M., D. S. Stevenson, C. E. Johnson, W. J. Collins, and M. G. Sanderson (2006), Tropospheric ozone and El Niño–Southern Oscillation: Influence of atmospheric dynamics, biomass burning emissions, and future climate change, *J. Geophys. Res.*, *111*, D19304, doi:10.1029/2005JD006849.

Doherty, R. M., et al. (2013), Impacts of climate change on surface ozone and intercontinental ozone pollution: A multi-model study, *J. Geophys. Res. Atmos.*, *118*, 3744–3763, doi:10.1002/jgrd.50266.

Eyring, V., T. Shepherd, and D. Waugh (2010a), SPARC report on the evaluation of chemistry-climate models, SPARC Report No. 5, WCRP-132, WMO/TD-No. 1526. [Available at http://www.atmosp.physics.utoronto.ca/SPARC.]

Eyring, V., et al. (2010b), Multi-model assessment of stratospheric ozone return dates and ozone recovery in CCMVal-2 models, *Atmos. Chem. Phys.*, *10*(19), 9451–9472, doi:10.5194/acp-10-9451-2010.

Eyring, V., et al. (2013a), Long-term ozone changes and associated climate impacts in CMIP5 simulations, *J. Geophys. Res.*, *118*(10), 5029–5060, doi:10.1002/jgrd.50316.

Eyring, V., et al. (2013b), Overview of IGAC/SPARC Chemistry-Climate Model Initiative (CCMI) community simulations in support of upcoming ozone and climate assessments, SPARC Newsletter no. 4, WMO-WRCP, pp. 48–66, Geneva, Switzerland. [Available at http://eprints.lancs.ac.uk/id/eprint/62147.]

Forster, P., et al. (2007), Changes in atmospheric constituents and in radiative forcing, in *Climate Change 2007: The Physical Science Basis. Contribution of Working Group I to the Fourth Assessment Report of the Intergovernmental Panel on Climate Change*, edited by S. Solomon et al., chap. 2, pp. 129–234, Cambridge Univ. Press, Cambridge, U. K., and New York.

Fusco, A. C., and J. A. Logan (2003), Analysis of 1970–1995 trends in tropospheric ozone at Northern Hemisphere midlatitudes with the GEOS-CHEM model, *J. Geophys. Res.*, *108*, 4449, doi:10.1029/2002JD002742.

Gillett, N. P., et al. (2011), Attribution of observed changes in stratospheric ozone and temperature, *Atmos. Chem. Phys.*, *11*(2), 599–609, doi:10.5194/acp-11-599-2011.

Guenther, A., et al. (1995), A global model of natural volatile organic compound emissions, *J. Geophys. Res.*, *100*(D5), 8873–8892, doi:10.1029/94JD02950.

Hess, P., and N. Mahowald (2009), Interannual variability in hindcasts of atmospheric chemistry: The role of meteorology, *Atmos. Chem. Phys.*, *9*(14), 5261–5280, doi:10.5194/acp-9-5261-2009.

Houweling, S., F. Dentener, and J. Lelieveld (1998), The impact of nonmethane hydrocarbon compounds on tropospheric photochemistry, *J. Geophys. Res.*, *103*(D9), 10,673–10,696, doi:10.1029/97JD03582.

Hsu, J., M. J. Prather, and O. Wild (2005), Diagnosing the stratosphere-to-troposphere flux of ozone in a chemistry transport model, *J. Geophys. Res.*, *110*, D19305, doi:10.1029/2005JD006045.

Johnson, C. E., D. S. Stevenson, W. J. Collins, and R. G. Derwent (2001), Role of climate feedback on methane and ozone studied with a Coupled Ocean-Atmosphere-Chemistry Model, *Geophys. Res. Lett.*, *28*(9), 1723–1726, doi:10.1029/2000GL011996.

Kawase, H., T. Nagashima, K. Sudo, and T. Nozawa (2011), Future changes in tropospheric ozone under Representative Concentration Pathways (RCPs), *Geophys. Res. Lett.*, *38*, L05801, doi:10.1029/2010GL046402.

Koumoutsaris, S., I. Bey, S. Generoso, and V. Thouret (2008), Influence of El Niño–Southern Oscillation on the interannual variability of tropospheric ozone in the northern midlatitudes, *J. Geophys. Res.*, *113*, D19301, doi:10.1029/2007JD009753.

Lamarque, J.-F., et al. (2010), Historical (1850–2000) gridded anthropogenic and biomass burning emissions of reactive gases and aerosols: Methodology and application, *Atmos. Chem. Phys.*, *10*(15), 7017–7039, doi:10.5194/acp-10-7017-2010.

Lamarque, J.-F., et al. (2013), The Atmospheric Chemistry and Climate Model Intercomparison Project (ACCMIP): Overview and description of models, simulations and climate diagnostics, *Geoscientific Model Dev.*, *6*(1), 179–206, doi:10.5194/gmd-6-179-2013.

Lang, C., D. W. Waugh, M. A. Olsen, A. R. Douglass, Q. Liang, J. E. Nielsen, L. D. Oman, S. Pawson, and R. S. Stolarski (2012), The impact of greenhouse gases on past changes in tropospheric ozone, *J. Geophys. Res.*, *117*, D23304, doi:10.1029/2012JD018293.

Langford, A. O., T. J. O'Leary, C. D. Masters, K. C. Aikin, and M. H. Proffitt (1998), Modulation of middle and upper tropospheric ozone at northern midlatitudes by the El Niño/Southern Oscillation, *Geophys. Res. Lett.*, *25*(14), 2667–2670, doi:10.1029/98GL01909.

Li, F., R. S. Stolarski, and P. A. Newman (2009), Stratospheric ozone in the post-CFC era, *Atmos. Chem. Phys.*, *9*(6), 2207–2213, doi:10.5194/acp-9-2207-2009.

Lin, S.-J., and R. B. Rood (1996), Multidimensional flux-form semi-Lagrangian transport schemes, *Mon. Weather Rev.*, *124*(9), 2046–2070, doi:10.1175/1520-0493(1996)124<2046:MFFSLT>2.0.CO;2.

Livesey, N. J., et al. (2011), Earth Observing System (EOS) Aura Micro-wave Limb Sounder (MLS) Version 3.3 Level 2 data quality and description document, *Tech. Rep.*, Jet Propulsion Laboratory California Institute of Technology, Pasadena, Calif.

Masui, T., K. Matsumoto, Y. Hijioka, T. Kinoshita, T. Nozawa, S. Ishiwatari, E. Kato, P. Shukla, Y. Yamagata, and M. Kainuma (2011), An emission pathway for stabilization at 6 W m^{-2} radiative forcing, *Clim. Change*, *109*(1-2), 59–76, doi:10.1007/s10584-011-0150-5.

McFarlane, N. A. (1987), The effect of orographically excited gravity wave drag on the general circulation of the lower stratosphere and troposphere, *J. Atmos. Sci.*, *44*(14), 1775–1800, doi:10.1175/1520-0469(1987)044<1775:TEOOEG>2.0.CO;2.

Meinshausen, M., et al. (2011), The RCP greenhouse gas concentrations and their extensions from 1765 to 2300, *Clim. Change*, *109*(1–2), 213–241, doi:10.1007/s10584-011-0156-z.

Nagashima, T., M. Takahashi, M. Takigawa, and H. Akiyoshi (2002), Future development of the ozone layer calculated by a general circulation model with fully interactive chemistry, *Geophys. Res. Lett.*, *29*(8), 1162, doi:10.1029/2001GL014026.

Nassar, R., J. A. Logan, I. A. Megretskaia, L. T. Murray, L. Zhang, and D. B. A. Jones (2009), Analysis of tropical tropospheric ozone, carbon monoxide, and water vapor during the 2006 El Niño using TES observations and the GEOS-Chem model, *J. Geophys. Res.*, *114*, D17304, doi:10.1029/2009JD011760.

Oman, L. D., J. R. Ziemke, A. R. Douglass, D. W. Waugh, C. Lang, J. M. Rodriguez, and J. E. Nielsen (2011), The response of tropical tropospheric ozone to ENSO, *Geophys. Res. Lett.*, *38*, L13706, doi:10.1029/2011GL047865.

Oman, L. D., A. R. Douglass, J. R. Ziemke, J. M. Rodriguez, D. W. Waugh, and J. E. Nielsen (2013), The ozone response to ENSO in Aura satellite measurements and a chemistry-climate simulation, *J. Geophys. Res.*, *118*, 965–976, doi:10.1029/2012JD018546.

Pozzoli, L., G. Janssens-Maenhout, T. Diehl, I. Bey, M. G. Schultz, J. Feichter, E. Vignati, and F. Dentener (2011), Re-analysis of tropospheric sulfate aerosol and ozone for the period 1980–2005 using the aerosol-chemistry-climate model ECHAM5-HAMMOZ, *Atmos. Chem. Phys.*, *11*(18), 9563–9594, doi:10.5194/acp-11-9563-2011.

Randel, W. J., and A. M. Thompson (2011), Interannual variability and trends in tropical ozone derived from SAGE II satellite data and SHADOZ ozonesondes, *J. Geophys. Res.*, *116*, D07303, doi:10.1029/2010JD015195.

Randel, W. J., and F. Wu (1996), Isolation of the Ozone QBO in SAGE II data by singular-value decomposition, *J. Atmos. Sci.*, *53*(17), 2546–2559, doi:10.1175/1520-0469(1996)053<2546:IOTOQI>2.0.CO;2.

Randel, W. J., and F. Wu (2007), A stratospheric ozone profile data set for 1979–2005: Variability, trends, and comparisons with column ozone data, *J. Geophys. Res.*, *112*, D06313, doi:10.1029/2006JD007339.

Randel, W. J., R. R. Garcia, N. Calvo, and D. Marsh (2009), ENSO influence on zonal mean temperature and ozone in the tropical lower stratosphere, *Geophys. Res. Lett.*, *36*, L15822, doi:10.1029/2009GL039343.

Rayner, N. A., D. E. Parker, E. B. Horton, C. K. Folland, L. V. Alexander, D. P. Rowell, E. C. Kent, and A. Kaplan (2003), Global analyses of sea surface temperature, sea ice, and night marine air temperature since the late nineteenth century, *J. Geophys. Res.*, *108*(D14), 4407, doi:10.1029/2002JD002670.

Roelofs, G.-J., and J. Lelieveld (2000), Tropospheric ozone simulation with a chemistry-general circulation model: Influence of higher hydrocarbon chemistry, *J. Geophys. Res.*, *105*(D18), 22,697–22,712, doi:10.1029/2000JD900316.

Sekiya, T., and K. Sudo (2012), Role of meteorological variability in global tropospheric ozone during 1970–2008, *J. Geophys. Res.*, *117*, D18303, doi:10.1029/2012JD018054.

Shapiro, M. A., H. Wernli, N. A. Bond, and R. Langland (2001), The influence of the 1997–99 El Niño Southern Oscillation on extratropical baroclinic life cycles over the eastern North Pacific, *Q. J. R. Meteorol. Soc.*, *127*(572), 331–342, doi:10.1002/qj.49712757205.

Son, S.-W., L. Polvani, D. Waugh, H. Akiyoshi, R. Garcia, D. Kinnison, S. Pawson, E. Rozanov, T. Shepherd, and K. Shibata (2008), The impact of stratospheric ozone recovery on the Southern Hemisphere westerly jet, *Science*, *320*(5882), 1486–1489, doi:10.1126/science.1155939.

Son, S.-W., et al. (2010), Impact of stratospheric ozone on Southern Hemisphere circulation change: A multimodel assessment, *J. Geophys. Res.*, *115*, D00M07, doi:10.1029/2010JD014271.

Stevenson, D. S., et al. (2006), Multimodel ensemble simulations of present-day and near-future tropospheric ozone, *J. Geophys. Res.*, *111*, D08301, doi:10.1029/2005JD006338.

Stevenson, D. S., et al. (2013), Tropospheric ozone changes, radiative forcing and attribution to emissions in the Atmospheric Chemistry and Climate Model Intercomparison Project (ACCMIP), *Atmos. Chem. Phys.*, *13*(6), 3063–3085, doi:10.5194/acp-13-3063-2013.

Sudo, K., and H. Akimoto (2007), Global source attribution of tropospheric ozone: Long-range transport from various source regions, *J. Geophys. Res.*, *112*, D12302, doi:10.1029/2006JD007992.

Sudo, K., and M. Takahashi (2001), Simulation of tropospheric ozone changes during 1997–1998 El Niño: Meteorological impact on tropospheric photochemistry, *Geophys. Res. Lett.*, *28*(21), 4091–4094, doi:10.1029/2001GL013335.

Sudo, K., M. Takahashi, J. Kurokawa, and H. Akimoto (2002), CHASER: A global chemical model of the troposphere 1. Model description, *J. Geophys. Res.*, *107*(D17), 4339, doi:10.1029/2001JD001113.

Sudo, K., M. Takahashi, and H. Akimoto (2003), Future changes in stratosphere-troposphere exchange and their impacts on future tropospheric ozone simulations, *Geophys. Res. Lett.*, *30*(24), 2256, doi:10.1029/2003GL018526.

Takemura, T., T. Nozawa, S. Emori, T. Y. Nakajima, and T. Nakajima (2005), Simulation of climate response to aerosol direct and indirect effects with aerosol transport-radiation model, *J. Geophys. Res.*, *110*, D02202, doi:10.1029/2004JD005029.

Thompson, A. M., et al. (2003a), Southern Hemisphere Additional Ozonesondes (SHADOZ) 1998–2000 tropical ozone climatology 1. Comparison with Total Ozone Mapping Spectrometer (TOMS) and ground-based measurements, *J. Geophys. Res.*, *108*(D2), 8238, doi:10.1029/2001JD000967.

Thompson, A. M., et al. (2003b), Southern Hemisphere Additional Ozonesondes (SHADOZ) 1998–2000 tropical ozone climatology 2. Tropospheric variability and the zonal wave-one, *J. Geophys. Res.*, *108*(D2), 8241, doi:10.1029/2002JD002241.

Thompson, A. M., J. C. Witte, H. G. J. Smit, S. J. Oltmans, B. J. Johnson, V. W. J. H. Kirchhoff, and F. J. Schmidlin (2007), Southern Hemisphere Additional Ozonesondes (SHADOZ) 1998–2004 tropical ozone climatology: 3. Instrumentation, station-to-station variability, and evaluation with simulated flight profiles, *J. Geophys. Res.*, *112*, D03304, doi:10.1029/2005JD007042.

Tilmes, S., et al. (2012), Technical Note: Ozonesonde climatology between 1995 and 2011: Description, evaluation and applications, *Atmos. Chem. Phys.*, *12*(16), 7475–7497, doi:10.5194/acp-12-7475-2012.

Voulgarakis, A., P. Hadjinicolaou, and J. A. Pyle (2011), Increases in global tropospheric ozone following an El Niño event: Examining stratospheric ozone variability as a potential driver, *Atmos. Sci. Lett.*, *12*(2), 228–232, doi:10.1002/asl.318.

Wallace, J. M., R. L. Panetta, and J. Estberg (1993), Representation of the Equatorial Stratospheric Quasi-Biennial Oscillation in EOF Phase Space, *J. Atmos. Sci.*, *50*(12), 1751–1762, doi:10.1175/1520-0469(1993)050<1751:ROTESQ>2.0.CO;2.

Wang, C. (2002), Atmospheric circulation cells associated with the El Niño–Southern Oscillation, *J. Clim.*, *15*(4), 399–419, doi:10.1175/1520-0442(2002)015<0399:ACCAWT>2.0.CO;2.

Watanabe, S., et al. (2011a), MIROC-ESM 2010: Model description and basic results of CMIP5-20c3m experiments, *Geoscientific Model Dev.*, *4*(4), 845–872, doi:10.5194/gmd-4-845-2011.

Watanabe, S., K. Sudo, T. Nagashima, T. Takemura, H. Kawase, and T. Nozawa (2011b), Future projections of surface UV-B in a changing climate, *J. Geophys. Res.*, *116*, D16118, doi:10.1029/2011JD015749.

Wesely, M. (1989), Parameterization of surface resistances to gaseous dry deposition in regional-scale numerical models, *Atmos. Environ.*, *23*(6), 1293–1304, doi:10.1016/0004-6981(89)90153-4.

WMO (1957), Meteorology—A three-dimensional science, *WMO Bull.*, *6*, 134–138.

Worden, J., S. S. Kulawik, M. W. Shephard, S. A. Clough, H. Worden, K. Bowman, and A. Goldman (2004), Predicted errors of tropospheric emission spectrometer nadir retrievals from spectral window selection, *J. Geophys. Res.*, *109*, D09308, doi:10.1029/2004JD004522.

Young, P. J., et al. (2013), Pre-industrial to end 21st century projections of tropospheric ozone from the Atmospheric Chemistry and Climate Model Intercomparison Project (ACCMIP), *Atmos. Chem. Phys.*, *13*(4), 2063–2090, doi:10.5194/acp-13-2063-2013.

Zeng, G., and J. A. Pyle (2003), Changes in tropospheric ozone between 2000 and 2100 modeled in a chemistry-climate model, *Geophys. Res. Lett.*, *30*(7), 1392, doi:10.1029/2002GL016708.

Zeng, G., and J. A. Pyle (2005), Influence of El Niño Southern Oscillation on stratosphere/troposphere exchange and the global tropospheric ozone budget, *Geophys. Res. Lett.*, *32*, L01814, doi:10.1029/2004GL021353.

Zeng, G., J. A. Pyle, and P. J. Young (2008), Impact of climate change on tropospheric ozone and its global budgets, *Atmos. Chem. Phys.*, *8*(2), 369–387, doi:10.5194/acp-8-369-2008.

Ziemke, J. R., and S. Chandra (1999), Seasonal and interannual variabilities in tropical tropospheric ozone, *J. Geophys. Res.*, *104*(D17), 21,425–21,442, doi:10.1029/1999JD900277.

Ziemke, J. R., S. Chandra, L. D. Oman, and P. K. Bhartia (2010), A new ENSO index derived from satellite measurements of column ozone, *Atmos. Chem. Phys.*, *10*(8), 3711–3721, doi:10.5194/acp-10-3711-2010.